EFFICIENT AIR FLOW CONTROL FOR REMOTE LASER BEAM WELDING

Paper 703

Achim Mahrle[1,2], Madlen Borkmann[2,1], Eckhard Beyer[1,2], Christoph Leyens[1,2], Michael Hustedt[3], Christian Hennigs[3], Alexander Brodeßer[3], Jürgen Walter[3], Stefan Kaierle[3]

[1] Fraunhofer IWS Dresden, Winterbergstraße 28, D-01277 Dresden, Germany

[2] Technische Universität Dresden, PO Box, D-01062 Dresden, Germany

[3] Laser Zentrum Hannover e.V., Hollerithallee 8, D-30419 Hannover, Germany

Abstract

Efficient air flow control plays a crucial role for the reliability of remote laser beam welding applications. Local air flows are helpful to suppress unfavorable interactions between laser radiation and welding fumes as a result of absorption and/or scattering effects. On the other hand, local and additional global flows have to be applied for emission control to protect optical components and workpieces from contamination and to avoid harmful air pollution of the atmosphere. However, the appropriate design of complex air flow systems under the additional condition of preferably low overall gas consumption is still a challenging task because a high number of decisive factors and a multitude of possible interactions complicate the pure empirical selection and positioning of suitable flow components and the adjustment of the numerous control parameters. This paper presents the results of a combined and complementary approach of experimental and theoretical investigations to meet these challenges. The experimental work was focused on the aspects of interaction mechanisms between the laser beam and the welding fume. Besides the characterization of process emissions some of the requirements of stable remote processing with maximum penetration depth are revealed. In contrast, the theoretical work describes a general methodology on how to support the optimization of the cabin air flow by means of Computational Fluid Dynamics (CFD) models in combination with Design-of-Experiments (DoE) approaches.

Introduction

Remote Laser Beam Welding (RLBW) can be considered as a particular laser beam welding process used for numerous applications in the automotive and sheet-metal processing industry [e.g. 1-5]. A common feature of those applications is the long working distance between the processing head with the focusing optics and the actual processing zone. Different benefits can be achieved by using this technology in comparison to common laser beam welding processes such as a high 2D and 3D flexibility, high welding speeds and fast positioning capabilities with different consecutive weld positions. However, there is often the need to realize those processes without any localized shielding gas supply in order to make the mentioned advantages fully exploitable. As a result, interactions between welding fumes not blown out of the laser beam path and the incident laser radiation become evident and can have a crucial impact on process reliability, penetration depth and weld seam quality.

Matsunawa and Ohnawa [6] proposed two major loss mechanisms of energy dissipation in the laser-induced plume, namely the photon absorption by electrons (Inverse Bremsstrahlung (IB absorption)) and interactions between the laser radiation and ultra-fine particles formed in the plume. It was shown that the main loss strongly depends on the wavelength of the incident laser beam. IB absorption plays the major role in CO_2 laser processing with an emission wavelength of 10.6 µm. In that case, the photon-electron inter-actions heat up the metal vapor to temperatures above 10^4 K. The plume becomes partially ionized and consequently absorbs a large part of the incident laser radiation. This well-known plasma shielding effect can only be suppressed by use of helium with its high ionization potential as a shielding gas. In contrast, plasmas are not thought to occur to a notable degree if solid-state laser sources with wavelengths around 1 µm are used under typical welding conditions [7]. Kawahito et al [8] have revealed by spectroscopic measurements that even in the case of fiber laser welding with 10 kW output power, the laser-induced plume mainly consists of metallic vapor from alloying elements of the processed materials and is not apparent in the ionized state. Accordingly, observed attenuation effects are not to be attributed to IB absorption, but to interactions between laser radiation and ultra-fine particles in the welding fume [9]. The mechanism of interaction strongly depends on particle size and composition and is based on absorption and scattering effects [10]. Greses et al [11] performed high-power Nd:YAG laser welding of mild steel under He, Ar and N_2 gas atmospheres and found the plume to be composed of particles with an average diameter less than 50 nm. Average values of the attenuation of a

probe laser beam ranged from 12 to 38% close to the top of the keyhole. Michalowski et al [12] presented in-situ measurement results of plume characteristics during welding of stainless steel. They found averaged particle sizes between 115 and 192 nm and determined the plume density to be in the range from 5 to $7x10^7$ cm^{-3}. It was concluded that for processing with Yb:YAG lasers, more than 30% of the laser energy can be lost due to scattering and absorption effects, if the plume is not removed from the beam path. Scholz et al [13] determined particle diameters in the range between 10 and 100 nm with a typical average size of about 30 nm for laser welding of stainless steel with a multi-mode fiber laser and without any process gas. In addition, fluctuations of the particle formation process were detected, giving rise to a non-negligible dynamical behavior of the interaction mechanisms of the incoming laser radiation with the vapor plume. It was also shown that the particle formation shows a strong dependence on process parameters such as welding speed and laser beam power [14]. The laser power attenuation during welding of stainless steel with a 1.6 kW fiber laser was found to be about 10%.

It is evident that the particle distribution in a laser-induced plume shows high spatial and temporal fluctuations. Shcheglov et al [15] revealed for fiber laser welding of mild steel plates that the welding plume has two different parts, each of them with its own dynamics, temperature and geometrical form. The lower part just above the processing zone has a bright glow and oscillates with frequencies of up to several kHz, whereas the upper part shows considerably weaker emission and corresponds to the propagation caustic of the applied laser beam, as far as its geometrical form is concerned. It was shown that the measured extinction coefficient in this upper part is much higher than in the lower part. Particle diameters were found to be in the range from 60 to 110 nm and the average attenuation was estimated to be about 12%. The reported attenuation levels seem to be not as high as expected to give a consistent explanation of the observed effects on penetration depth in welding experiments. However, it has to be considered that the axial beam path through the plume is longer than the way a lateral probe beam travels through this medium. In addition, it is expected that fluctuations of the beam power also have a strong impact on keyhole behavior and weld penetration. It seems to be obvious that attenuation effects by photon-particle interactions become particularly serious in welding applications with long focal distances such as remote laser beam welding. Local air flows used to clean the beam path are considered to be very helpful to suppress the described attenuation effects, but under conditions of series production, it is very important to apply additional local and global air flows to protect optical components and workpieces from contaminations with weld fume residuals and to avoid harmful air pollutions of the atmosphere, taking into account the requirement of preferably low overall gas consumption. It was tried to address these aspects by a combination of experimental and theoretical work. The performed experimental investigations describe some of the pre-requirements of reliable laser beam welding with maximal penetration depth, whereas the theoretical part gives some insights into the sophisticated relationships and dependencies concerning air flow control for laser welding applications.

Experimental Work

A test cabin was designed that enabled practical welding experiments under variation of the air flow conditions. Exterior and interior views of the developed station are shown in Figures 1 and 2. The cabin with a spatial volume of about 1.6 m^3 is well-equipped with several air flow components, including local and global flat-jet fan nozzles, local and global air extraction components and an air-knife to protect the processing optics. Each of these components offers various settings with respect to spatial position, orientation, outflow aperture, and flow rate.

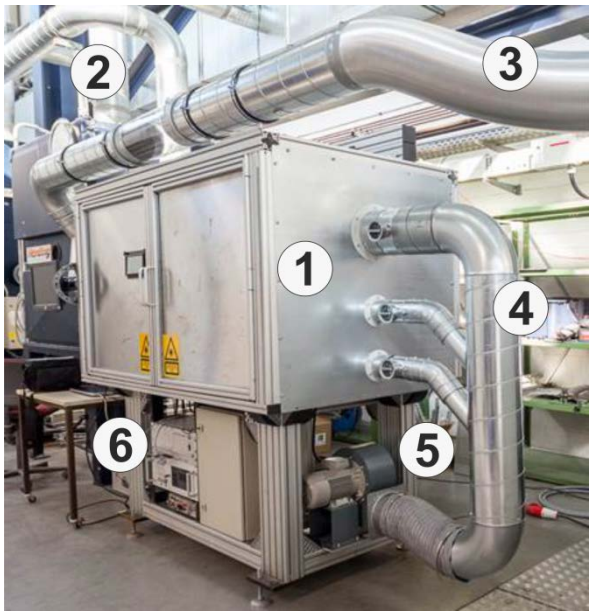

Figure 1: Exterior view of the test cabin: Enclosure (1), measuring cell for particle analysis (2), suction air pipe (3), supply air pipe (4), fan (5) and control units (6).

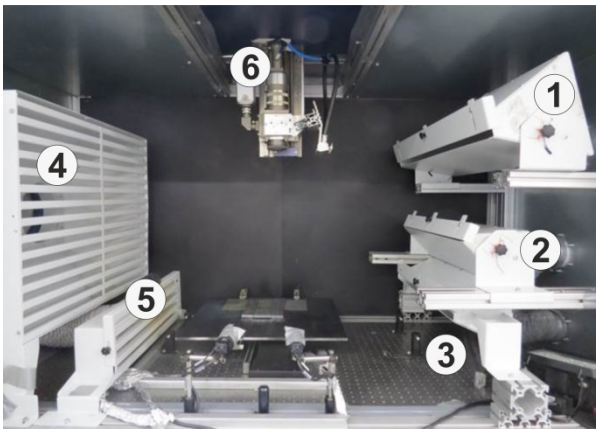

Figure 2: Interior view of the test cabin: global air supply (1), local air supply I (2), local air supply II (3), global exhaust air funnel (4), local exhaust air funnel (5), and beam optics (6).

Bead-on-plate welding trials were performed within the test cabin for thick-section mild steel plates (carbon steel ASTM A284, thickness 10 mm) by using a multi-mode fiber laser system with an applied optical output power of 3 kW and a focal diameter of 300 µm. Figure 3 shows the weld fume distributions under processing conditions and corresponding weld seam geometries for welding trials without any and with basic air flow control. In the case without any air flow, the effect of beam attenuation and reduced penetration depth is much more pronounced, and the weld seam geometry here even shows features of a transition to a conduction-mode welding regime.

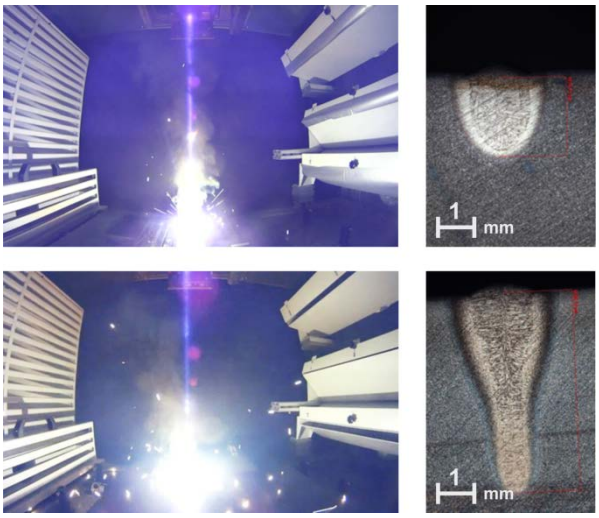

Figure 3: Weld fume distribution and corresponding weld seam geometries. Top: without any air flow. Bottom: with basic air flow. Welding parameters: laser power 3 kW, welding speed 2 m/min, focus diameter 300 µm, mild steel.

By applying the lateral air flow, the penetration depth increases by a factor of about 2.5. It is worthwhile to note that the plume size in lateral direction seems to be extended in the case with basic air flow control, i.e. the observable shape and size of the plume does not allow direct conclusions with respect to the strength of detrimental interactions. However, as proven by the increased penetration depth of the weld seam, it is concluded that the composition and properties of the weld fume are strongly affected by the air flow. It is also obvious that the plume consists of different parts as already described by Shcheglov et al [15]. Besides the brightly shining area just above the focusing area of the laser beam, there is a second zone that corresponds to the beam caustic geometry. It has be noted that both regions are present without and with air flow control. From a practical point of view, it is important to have knowledge about the magnitude of local air flow velocities that are needed to blow the plume away from the processing zone and the beam path. For that purpose, the local air flow velocities, measured by an anemometer and controlled by the flow rate in preliminary experiments without welding, were varied in the range from 1 to 10 m/s. It was revealed that the maximum penetration depths were already achieved at flow velocities of about 2 m/s. Higher velocities do not have any beneficial impact on the weld penetration and should be avoided. The analysis of the particle size distribution of the welding fumes by the use of an Electrical Low-Pressure cascade Impactor (ELPI^{TM}) revealed that 90% of the captured particles have dimensions smaller than 300 nm, see Figure 4. It can be concluded for this range of particle sizes that the attenuation of the laser radiation might depend on both, absorption and scattering effects. From the Rayleigh theory that describes these effects as a function of the particle radius, it is known that the scattering effect increases with particle size and becomes dominant for particle diameters above about 180 nm for an emission laser wavelength of ~ 1 µm [16].

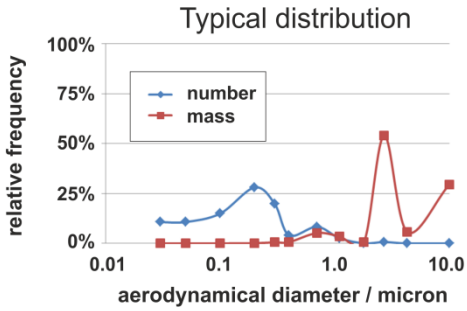

Figure 4: Typical measured particle size distribution (number and mass frequency) for fiber laser welding of mild steel plates with 3 kW laser power and a welding speed of 2 m/min.

Additional experimental investigations were performed in order to determine the tolerable plume height or interaction length that still allows for reaching the maximal penetration depth under the specified welding conditions. For that purpose, an adjustable cover sheet was placed between the beam optics and the workpiece with the processing zone. This sheet contains a small drill hole as passage for the incident laser radiation. Above the sheet, a cross-jet blows the fume away from the beam path, whereas underneath the sheet, the fume remains unaffected. Thus, the effective interaction length of laser radiation and weld fume is fixed by the distance of the cover sheet from the processing zone. It was found that a distance of up to 15 cm is acceptable to obtain welding results without detrimental effects on the weld penetration for this particular configuration [17]. However, it has to be stated that such a setup might influence the weld fume distribution and lead to an overestimation of the acceptable real plume height.

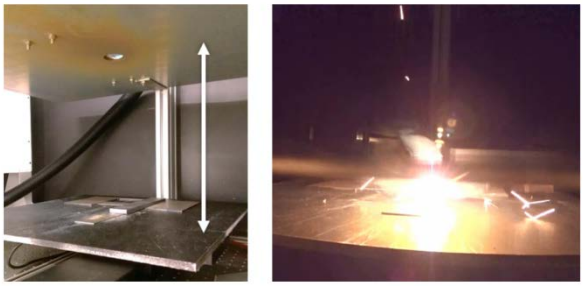

Figure 4: Determination of acceptable plume heights by a setup with an adjustable cover sheet.
Left: setup. Right: welding process.

Numerical Investigations

The gas flow inside the test cabin with several flow components depends on a high number of influencing factors such as flow rates, distances of the air flow components to the processing zone as well as orientation angles and outflow apertures of the flat-jet nozzles used. Interactions between different parameter settings can hardly be revealed by experimental means and the determination of an optimal parameter set requires a profound theoretical analysis. For that purpose, a Computational Fluid Dynamics (CFD) model of the test cabin was developed using the commercial software package ANSYS Fluent. This CFD model should enable an extensive virtual parameter study. Figure 5 shows the geometrical model of the test cabin that exactly corresponds in size and shape to the experimental design as shown in Figs. 1 and 2 with consideration of the symmetrical arrangement of all of the applied components with respect to a symmetry plane. The mesh typically consists of 3.5 million elements. The computation of the cabin flow is realized by a numerical solution of the Reynolds-Averaged Navier-Stokes (RANS) equations in combination with the k-ε turbulence model and the equation of state of ideal gas mixtures. Characteristic simulation times of particular parameter constellations amount to 3 – 5 hours under the assumption of a quasi-stationary state of the flow distribution. The time-dependent behavior can also be simulated, but with much higher computational efforts.

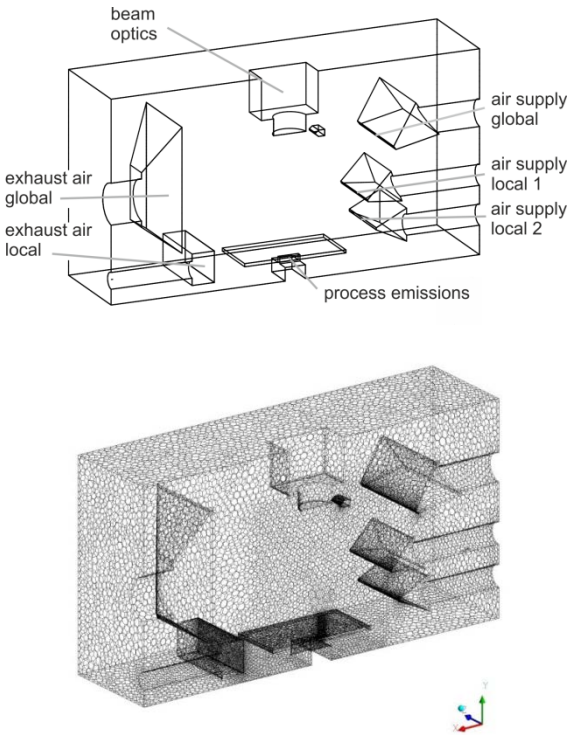

Figure 5: Geometrical model of the test cabin with applied flow components (top) and polyhedral mesh of the cabin with 3.5 million elements (bottom).

The model was not intended to describe the interactions between laser radiation and the nanoscaled particles present in the welding fume. This issue seems to be necessarily out of focus for an application-oriented model and has to be considered as a topic of further fundamental research. Instead, an adapted approach was applied to consider the process emissions as metallic vapor flowing into the test cabin by an aperture that corresponds to the keyhole diameter of a laser welding process. Typical inflow velocities of this vapor flow are in the range of 100 to 200 m/s. These values correspond to experimentally measured vapor velocities above the keyhole in deep penetration welding [18]. Exemplarily, Figure 6 shows a computed velocity field for a particular parameter configuration.

The metal vapor is mixed together with the ambient air, and the computed metal vapor concentration within the processing zone and along the beam path can be used as a criterion to evaluate the effectiveness of different parameter setups of the cabin air flow. In fact, the 1% isoline of the metal vapor concentration along the beam axis (called emission height) was determined. This quantity is sensitive to parameter variations of the cabin flow and was used as the response for parameter variations. It is suggested that the intensity of particle-beam interactions do correlate with the local metal vapor concentration because the particle formation mechanisms are thought to be closely related to the presence of metal vapor.

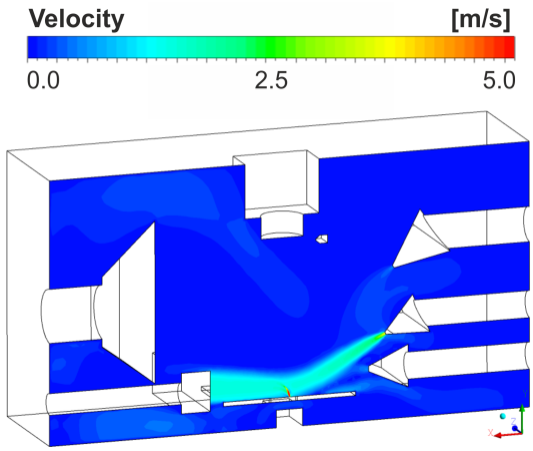

Figure 6: Example of a computed velocity distribution of the cabin flow.

The system behavior of the cabin flow was investigated extensively by means of Design-of-Experiment (DoE) methods. In a first phase, a screening design with consideration of 19 factors (emission vapor rates, orientation angles, outflow apertures, and inflow velocities of supply air components, pressure differences and characteristic dimensions of exhaust components) was performed [19]. Each of these factors was considered on two levels (minimum and maximum value). The aim of this study was the identification of the most vital factors of air flow control. Based on a fractional factorial design (minimum-run-design), the results of 192 different parameter constellations were analyzed. In summary, 6 of the 19 investigated factors were identified as the most vital ones, namely the orientation angle of the global air supply (factor A), the gap height of the global air supply (factor B), the flow rate of the global air supply (factor C), the flow rate of the local air supply I (factor D), the flow rate of the local air supply II (factor E), and the flow rate of the metal vapor emission (factor F). The latter was identified as the most important factor. Effects and interactions of these 6 factors were investigated in a second phase on the base of a full factorial design. The purpose of this stage of investigation was to derive a statistically reliable regression model that describes effects of these factors on the emission height as well as relevant interactions between these factors. However, the full factorial two-level design (linear model) as used initially was not adequate to describe the inherent dependencies with sufficient statistical validation. As a consequence, a response-surface multi-level design was applied with 157 numerical runs in total in order to get a statistically reliable cubic regression model for the emission height (response) with more than 40 significant effects and interactions [20]. Figure 7 shows the relative strengths of the 20 most crucial factors and interactions in terms of their coefficients in a normalized regression model. Negative effects increase the emission height whereas positive effects decrease the emission height. The results emphasize the sophisticated behavior of the gas flow in the test cabin considered here. In addition, it must be concluded that an analysis and discussion of separately investigated effects as commonly practiced by one-factor-at-a-time (OFAT) methods cannot be expected to be a promising approach, i.e. the system behavior must always be considered as a whole.

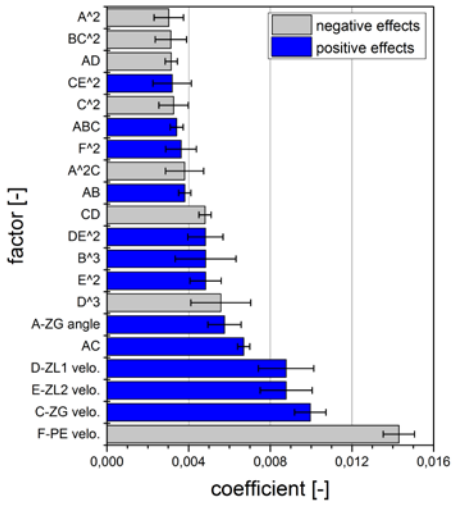

Figure 7: Relative strength of factors and factor-factor interactions influencing the emission height of the metal vapor in terms of their coefficients in the normalized regression model.

The derived cubic regression model describes the relationships between the selected parameters of the air flow control and the responses (emission height) very precisely, i.e. the emission height as decisive response can be calculated using this regression model as a function of given parameter values in the investigated parameter space. This type of calculation is very fast

and there is no need to make further flow field computations using the time-consuming numerical CFD model. In addition, statistical DoE-software supports the identification of optimal parameter constellations by corresponding algorithms. Using this capability, target criteria of an acceptable emission height at minimized overall gas consumption were specified. As the gas consumption is determined by the flow rates of the air supply components, the optimization function (called desirability in statistics as the overall measure of success for simultaneous optimization of multiple responses [21]) is shown as a function of local and global air supply in Figure 8. The target value of the emission height was assumed to be 20 mm for these calculations. It is obvious that the optimum is very sensitive to the flow rate of the local air supply. Deviations of the velocity of the local air supply from the optimal value give rise to a strong decrease of the desirability value. This is reasoned by the fact that too low values of the local velocity are not able to ensure the acceptable emission height. On the other hand, too high values might reduce the emission height under the specified value at unnecessary increased rates of gas consumption.

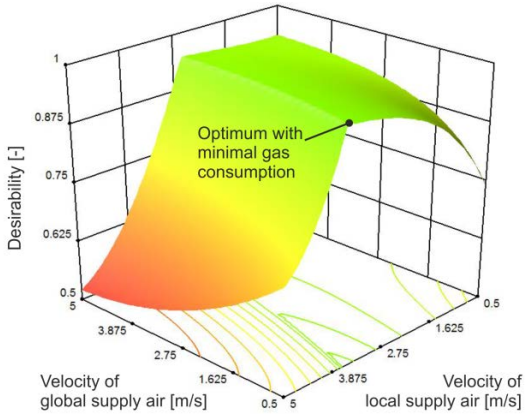

Figure 8: Optimization potential of the cabin air flow as a function of the global and local air supply flow rate.

CFD models as proven by a multitude of applications are commonly very accurate in describing the pressure and velocity fields of gas flows under the given boundary conditions. However, it was found out by experimental measurements that the agreement between experimental and numerical velocity profiles at particular positions inside the cabin was not as good as expected and additional computational efforts have been made to find out reasons for the detected deviations. As the most promising step, the applied boundary conditions defined for inflow and outflow apertures of the applied individual flow components were checked, revealing some interesting insights into design aspects of these components. As an example, the geometry of the used flat-jet nozzle type is shown in Figure 9. It consists of a tubular inlet area, a funnel-shaped outer geometry, and a perforated sheet that is thought to homogenize the velocity profile through the outflow aperture (4).

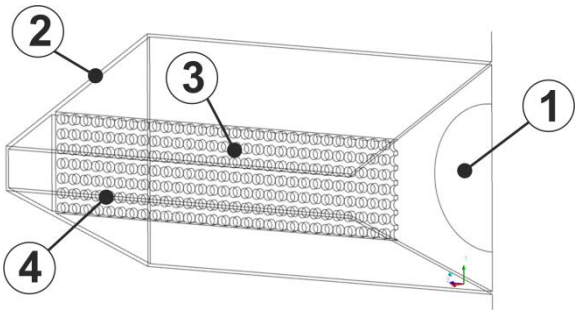

Figure 9: Half-section of the applied flat-jet nozzle type with tubular air supply (1), funnel-shaped outer geometry (2), perforated internal sheet (3) and rectangular outflow aperture.

The simulation of the gas flow through this component has demonstrated that the outflow velocity profile is far from being homogeneous as assumed as a boundary condition for the simulation of the cabin flow. Figure 10 shows the pathways of the streamlines as well as the normal velocity distribution of a plane that is arranged parallel to the outflow plane of the flat-jet nozzle at a distance of 300 mm. It is obvious that the main stream of the gas flow is deviated to the sides which show pronounced local maxima of the flow velocity. The further numerical analysis has demonstrated that the profile of the flow out of the nozzle depends on a number of geometrical quantities such as (i) the outflow aperture (gap height), (ii) the nozzle angle and/or nozzle depth, (iii) the position of the perforated sheet, (iv) the size, arrangement and number of the drilled holes of the perforated sheet, (v) the position, size and shape of the air supply channel, and (vi) the effect of possible installations and junctions of the supply pipes. As an example, Figure 11 shows the effect of a changed hole diameter of the perforated sheets on the flow profile, again at a distance of 300 mm from the outflow plane of the nozzle.

It can be concluded that the reliable simulation of the cabin gas flow usually requires an evaluation of the flow behavior of each of the applied components in order to justify particular boundary conditions made for the global cabin model. In order to reach a high accuracy level, the individual components should be separately investigated first. An optimization of these components should be sought in dependence on their specific function.

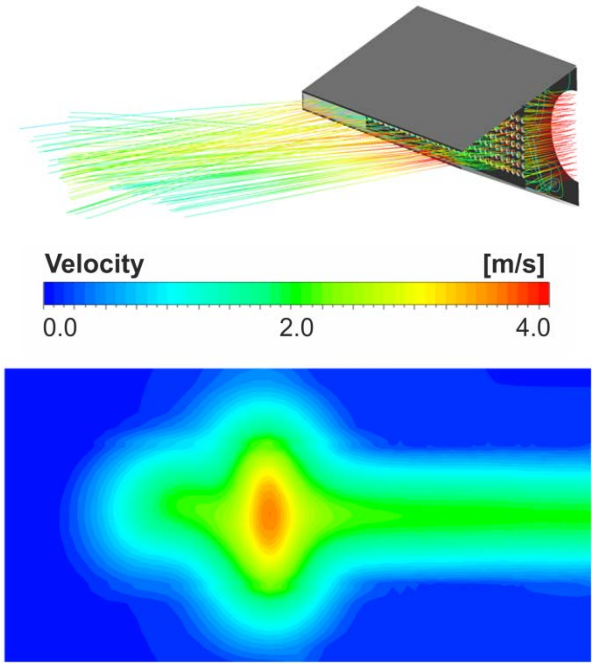

Figure 10: Streamlines and flow profile of the outflow of a flat-jet nozzle at a distance of 300 mm from the outflow plane of the nozzle. Hole diameter 8 mm.

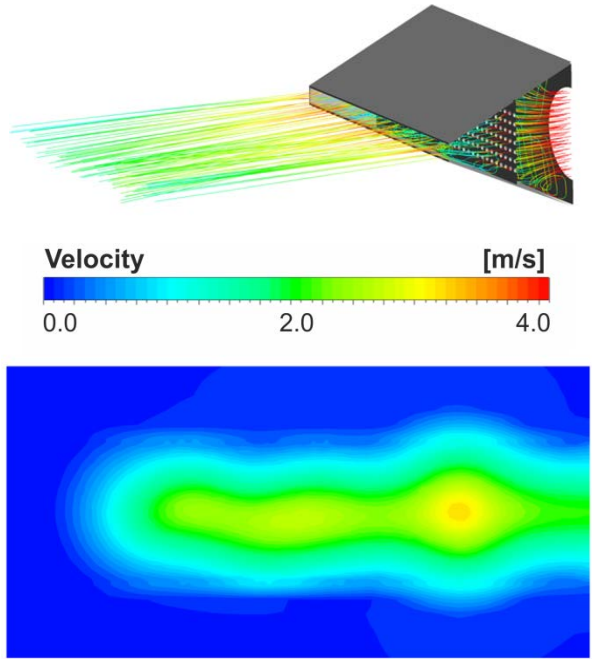

Figure 11: Streamlines and flow profile of the outflow of a flat-jet nozzle at a distance of 300 mm from the outflow plane of the nozzle. Hole diameter 5 mm.

This methodology is particularly considered as important for the inlet components applied here, whereas the outflow velocity profiles are self-consistently computed for outlet components as a function of the outlet pressure. The optimized flow profiles through the inflow apertures can then be used as boundary conditions for the cabin model. Using this model, the interplay between individual components can be simulated under the requirement of an efficient air flow control for remote laser beam welding processes. This sequential methodology ensures that the numerical efforts for extensive parameter studies remain tolerable.

Summary and Discussion

Conditions and characteristics of efficient air flow control for remote laser beam welding with high-power solid-state laser sources have been elucidated. The most important findings and conclusions are summarized as follows:

- A weld fume is formed during solid-state laser welding that is capable to have a crucial impact on process stability and weld seam quality.
- Most probably, detrimental effects result from interactions between the incident laser radiation and small particles being formed in the processing zone and causing absorption and scattering of laser radiation. However, inherent interaction mechanisms are not completely understood, hardly observable by experimental means and difficult to describe by theoretical approaches. Most accepted hypotheses are based on Rayleigh and Mie scattering theories.
- The analysis of particle size and density during fiber laser welding of mild steel plates revealed a high number of particles smaller than 300 nm in diameter with an overall probability of 90%. However, the highest mass probability with over 50% is reached by particles with about 2 – 4 µm in diameter. It is expected that a non-uniform particle distribution determines the interaction mechanisms taking place in the processing zone.
- The effective strength of the interactions between welding fume and laser radiation depends on the axial extension of the plume (plume height). Under the considered processing conditions (3 kW laser power, 2 m/min welding speed, mild steel), a plume height of about 150 mm was acceptable, without significant reduction of the weld penetration or impairment of weld quality.
- From a practical point of view, there is a simple approach to suppress detrimental interactions between a laser beam and a weld fume by blowing away the plume using local fans.

- A cross-flow at velocities equal to or larger than 2 m/s above the processing zone is sufficient to suppress detrimental interactions between laser beam and welding plume. Higher flow velocities are acceptable but unnecessarily increase the gas consumption. It is expected that many air flow systems in practice are oversized.
- Blowing away the welding fume by local fans without appropriate exhaust components give rise to an increased pollution of the cabin air and causes contamination of optical components, workpieces and cabin walls.
- Pollution of the cabin air with residual emissions of the welding process such as metallic oxides are harmful and may sometimes be carcinogenic in dependence on the materials being welded.
- An effective air flow control, taking into account different aspects of the cabin air flow is a challenging task because local and global flows in closed cabins often interact, and changed parameters of one component may affect the flow characteristics of the other components.
- In addition, the flow characteristics of individual components might not be well understood, and the real gas flow can deviate from the expected flow behavior.
- The flow characteristics of individual air flow components as well as the characteristics of the whole cabin flow depend on a high number of influencing factors. The comprehensive study of cause-effect relationships reveals a high number of interactions between those factors, which are hardly to be controlled empirically. Furthermore, it is a challenge to supervise the cabin air flow by experimental means.
- A promising remedy is the computer-aided design of cabin flows by means of Computational Fluid Dynamics (CFD) models. These models are capable to describe gas flows very precisely, provided the boundary conditions, i.e. the flow characteristics of individual components applied, are well captured.
- Using Design-of-Experiment (DoE) methods, the cabin flow can be characterized comprehensively by means of appropriate regression models that consider the effects of individual factors as well as interactions between factors. Based on these regression models, an optimization taking into account multiple criteria (warranty of process stability, avoidance of air pollution and contamination of optical components, minimum gas consumption) can be reached very effectively.

The performed work deepened the knowledge of remote laser beam welding problems and issues in a considerable way. The experimental techniques applied have provided significant insights into the mechanisms of interactions between laser radiation and welding fumes and showed some of the conditions for a stable welding process. The numerical analysis demonstrated the complexity of inherent dependencies for an efficient air flow control and revealed some of the challenges the users are faced with when an optimization of the air flow control is wanted to achieve. It can be summarized that trial and error approaches are not suitable to find optimal solutions because of the high number of influencing factors and interactions. With respect to the accuracy of the computational methods it was revealed that the assumption of simplistic boundary conditions for the applied flow components have to be verified first as exemplarily shown for inflow nozzles from the flat-jet type. Building such sub-models seems to be necessary to get reliable models of the whole cabin flow.

General rules for the design of industrial processing cabins can hardly be derived from the performed study because the characteristics of particular designs, the spatial and temporal conditions, the type of applied air-flow components and the peculiarities of the specific welding applications have to be taken into account for a profound analysis.

References

[01] F. Oefele (2012). Remote-Laserstrahlschweißen mit brillanten Laserstrahlquellen, Dissertationsschrift, Technische Universität München, München (Germany), 218 pp.

[02] A. Fysikopoulos, G. Pastras, J. Stavridis, P. Stavropoulos, G. Chryssolouris (2016). On the performance evaluation of remote laser welding process: an automative case study, Procedia CIRP, 41, 969-974.

[03] C. Roos, M. Schmidt (2014). Remote laser welding of zinc-coated sheets in an edge lap configuration with zero gap, Physics Procedia, 56, 535-544.

[04] P. Kah, J. Lu, J. Martikainen, R. Suovanta (2013). Remote laser welding with high power fiber lasers, Engineering, 5, 700-706.

[05] J. Lu, V. Kujanpää (2013). Review study on remote laser welding with fiber lasers, Journal of Laser Applications, Vol. 25, No. 3, paper 052008 (7 pp).

[06] A. Matsunawa, T. Ohnawa (1991). Beam-plume interaction in laser material processing, Transactions of JWRI, publ. by Welding Research Institute of Osaka University, 9-15.

[07] C.H.J. Gerritsen, C.A. Olivier (1996). Optimization of plasma/plume control for high-power Nd:YAG laser welding of 15 mm thickness C-Mn steels, Proc. of the 6th Int. Conf. on Trends in Welding Research, Pine Mountain (GA, USA), April 2002, Callway Gardens Report, 15-19.

[08] Y. Kawahito, N. Matsumoto, M. Mizutani, S. Katayama (2008). Characterization of plasma induced during high-power fibre laser welding of stainless steel, Science and Technology of Welding and Joining, Vol. 13, No. 8, 744-748.

[09] Y. Kawahito, K. Kinoshita, N. Matsumoto, M. Mizutani, S. Katayama (2008). Effect of weakly ionized plasma on penetration of stainless steel weld produced with ultra-high power density fibre laser, Science and Technology of Welding and Joining, Vol. 13, No. 8, 749-753.

[10] F. Hansen, W.W. Duley (1994). Attenuation of laser-radiation by perticles during laser materials processing, Journal of Laser Applications, Vol. 6, 137-143.

[11] J. Greses, P.A. Hilton, C.Y. Barlow, W.M. Steen (2004). Plume attenuation under high power Nd:YAG-aluminum-garnet laser welding, Journal of Laser Applications, Vol. 16, No. 1, 9-15.

[12] A. Michalowski, A. Heß, A. Ruß, F. Dausinger (2007). Plume attenuation under high-power Yb:YAG laser material processing, Proc. 4th Int. WLT-Conference on Lasers in Manufacturing, LIM 2007, Munich, 357-361.

[13] T. Scholz, K. Dieckmann, A. Ostendorf (2013). Investigation of the formation of nanoparticles during remote welding, Physics Procedia, 41, 90-97.

[14] T. Scholz, K. Dieckmann, A. Ostendorf (2014). Impact of process parameters on the laser-induced nanoparticle formation during keyhole welding under remote conditions, Physics Procedia, 56, 477-485.

[15] P.Y. Shcheglov, A.V. Gumenyuk, I.B. Gornushkin, M. Rethmeier (2013). Vapor-plasma plume investigation during high-power fiber laser welding, Laser Physics, Vol. 23, paper 016001 (7 pp).

[16] C.F. Bohren, D.R. Huffmann (1998). Absorption and Scattering of Light by Small Particles, Weinheim: Wiley-VCH vergal GmbH.

[17] J. Walter, C. Hennigs, M. Hustedt, S. Kaierle, M. Borkmann, A. Mahrle, E. Beyer (2016). Luftströmungsführung in Bearbeitungsstationen zum Remote-Laserstrahlschweißen – Teil 1: Experimente zur Anlagenoptimierung, 24. Fachtagung "Experimentelle Strömungsmechanik", Cottbus (Germany), 6-8. September 2016.

[18] E. Beyer (1995). Schweißen mit Laser, Berlin – Heidelberg: Springer, p. 87.

[19] M. Borkmann, A. Mahrle, E. Beyer, J. Walter, C. Hennigs, M. Hustedt, S. Kaierle (2015). Optimierte Luftströmungsführung beim Remote-Laserstrahlschweißen. Teil II: Numerische Untersuchungen, 23. Fachtagung "Lasermethoden in der Strömungsmesstechnik", Dresden (Germany), 8-10 September 2015.

[20] M. Borkmann, A. Mahrle, E. Beyer, C. Hennigs, M. Hustedt, J. Walter, S. Kaierle (2016). Luftströmungsführung in Bearbeitungsstationen zum Remote-Laserstrahlschweißen – Teil 2: Simulationen zur Anlagenoptimierung, 24. Fachtagung "Experimentelle Strömungsmechanik", Cottbus (Germany), 6-8. September 2016.

[21] M.J. Anderson, P.J. Whitcomb (2005). RSM Simplified – Optimizing Processes Using Response Surface Methods for Design of Experiments, Boca Raton (FL, USA): Taylor & Francis Group, pp. 124-25.

Acknowledgements

The work presented here was performed in close collaboration by the Laser Zentrum Hannover e.V. (LZH) and the Fraunhofer IWS Dresden as part of the publicly funded research project "Steigerung von Prozessstabilität und Schweißnahtqualität beim Remote-Laserschweißen durch gezielte Strömungsführung mittels Anlagenadaption" (RemoStAad), with the reference number IGF 18149 BG. The authors acknowledge the financial and administrative support by the Bundesministerium für Wirtschaft und Energie (BMWi), the Arbeitsgemeinschaft industrieller Forschungsvereinigungen "Otto von Guericke e.V." the Forschungskuratorium Maschinenbau e.V. (FKM), the Verein Deutscher Maschinen und Anlagenbau (VDMA), and the Forschungsvereinigung Schweißen und verwandte Verfahren e.V.